Packaging Technology of IPMs for Hybrid Vehicles

GOHARA Hiromichi * ARAI Hirohisa ⁑ MOROZUMI Akira *

ABSTRACT

Intelligent power modules (IPMs) control the power of hybrid vehicles. IPMs are needed to be downsized and lightweight due to the request for fuel efficiency and comfort. To achieve these requirements, Fuji Electric has developed a high-capacity IPM for hybrid vehicle integrated buck-boost converter and two inverters. This time, we have developed cooling design technology and high-strength solder technology, which realize a direct liquid cooling module with an integrated aluminum heat sink. This product has achieved a product volume reduction of 30% and mass reduction of 60% compared with the conventional indirect cooling structures and high reliability required for vehicles. The mass production of the product has already begun.

1. Introduction

Prevention of global warming and effective use of resources are gaining importance as activities shared by all the countries of the world. In the automobile industry, the development of hybrid electric vehicles (HEVs) and electric vehicles (EVs) are accelerating. In this situation, Fuji Electric started mass production of intelligent power modules (IPMs) for HEVs in December 2012. This product integrates inverter units for controlling two motors and a buck-boost converter unit, and realizes the high output required for HEVs with a compact and lightweight module. We have used low-loss sixth-generation insulated gate bipolar transistors (IGBTs) and free-wheeling diodes (FWDs) for high efficiency. Direct liquid cooling structure was realized to enhance the cooling performance. Lightweight aluminum was applied to a heat sink to reduce the weight.

In addition, it is equipped with a high-precision buck-boost control function and high-precision chip temperature communication function besides the IBGT protection function.

This paper presents an overview of the product and describes two new packaging technologies. One is cooling design technology with the direct liquid cooling structure and the other is high-strength soldering technology that allows solder bonding between aluminum, which has a large coefficient of thermal expansion, and an insulating substrate.

2. Overview of Product

Figure 1 shows the external picture of the developed IPM and Fig. 2 the circuit configuration. With conventional IPMs, it was common that the inverter unit–power drive unit (PDU)–and buck-boost converter unit–voltage control unit (VCU)–are mounted on them with configuring different modules for respective functions. This product is an all-in-one package integrating the two inverter units, buck-boost converter and controller (gate driver) and achieves high output with a small and lightweight module.

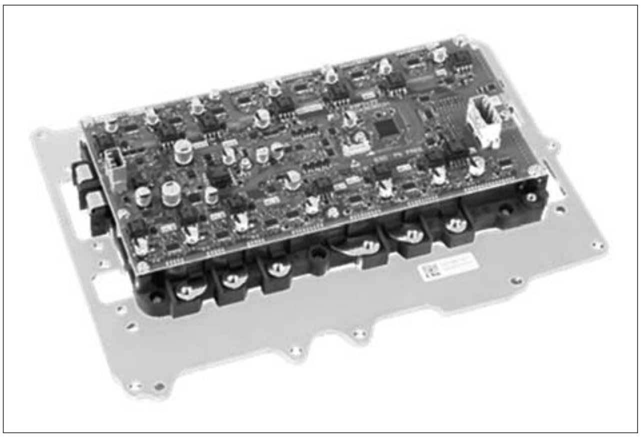

Fig.1 IPM for HEV

2.1 Structural characteristics

The following describes the major structural characteristics.

(a) 1,200 V/500 A, 14 in 1 IPM
(b) Size: L340×W233×H70 (mm) (30% volume reduction from previous product)
(c) Mass: 3.6 kg (60% mass reduction from previous product)
(d) High cooling performance due to aluminum direct liquid cooling structure
(e) Mounted with low-loss sixth-generation IGBTs

* Corporate R&D Headquarters, Fuji Electric Co., Ltd.
⁑ Electronic Devices Business Group, Fuji Electric Co., Ltd.

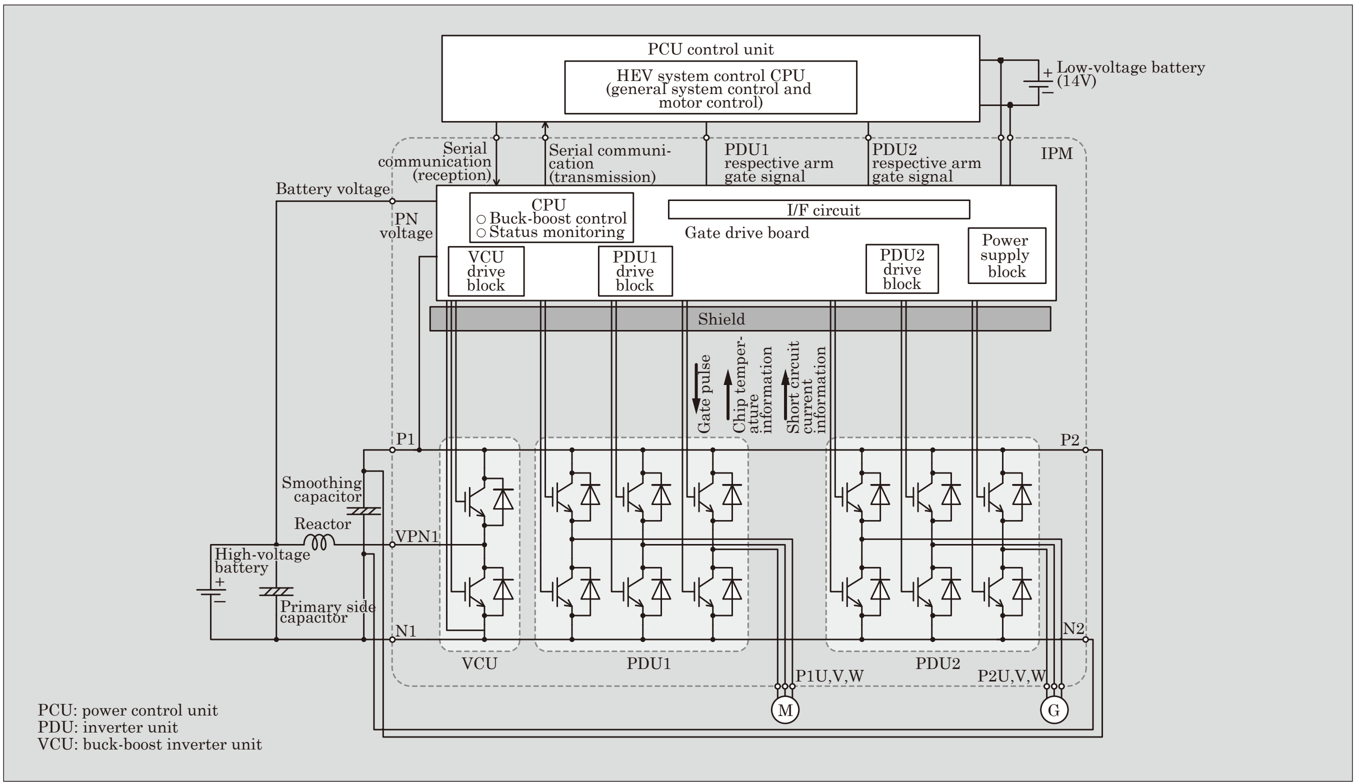

Fig.2 IPM circuit configuration

and FWDs

A gate drive board is placed on the module to realize the high functionality as described in Section 2.2

2.2 Functional characteristics

The following describes the major functional characteristics.

(a) Power supply for respective outputs generation from low-voltage battery

Insulated power supply with 18 outputs including IGBT driver power supply is provided.

(b) Built-in protection function for short-circuiting, overheat and power supply voltage drop

(c) High-precision IGBT chip temperature communication

(d) Gathering of operating status information and serial communication by integrated CPU

IPM operating status information and alarm information from the IGBT drive circuits are used for linking with the upper level to handle abnormal statuses.

(e) Buck-boost control by high-precision voltage measurement of high-voltage battery

The high-voltage battery voltage and PN voltage are monitored by the integrated CPU with instructions from the upper level for constant voltage control. For voltage measurement, high precision is achieved by CPU correction.

This product helps to achieve the industry's best fuel efficiency of high-output HEVs*[1].

3. Characteristics of Direct Liquid Cooling Structure

3.1 Direct liquid cooling structure with aluminum heat sink

Figure 3 describes the cross-section structure of the power module unit. Figure 3 (a) shows an indirect liquid cooling structure, which is a common cooling method. With the focus on cooling performance, this structure uses copper for the base plate. However, thermal grease with a low thermal conductivity of 1 W/(m・K) was used for thermal bonding between the base plate and the heat sink, which caused the thermal resistance to increase. For this reason, cooling performance was insufficient in the environment of a vehicle engine compartment with high ambient temperature. In addition, the high specific gravity of copper led to an increase in the mass of the power module unit, and this hindered the improvement of the vehicle's fuel ef-

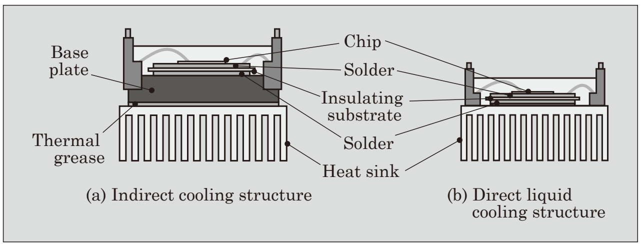

Fig.3 Cross-section structure of power module unit

*1: Highest fuel efficiency in class as of January 2013.

Table 1 Fundamental physical properties of insulating substrate and heat sink materials

	Thermal conductivity [W/(m·K)]	Thermal expansion coefficient (ppm/K)	Density x 10^{-6} (kg/mm^3)
Silicon nitride	90	3.4	3.3
Aluminum nitride	170	4.6	3.3
Copper	393	16.5	9.0
Aluminum	170	23.5	2.7

ficiency.

Figure 3 (b) shows a direct liquid cooling structure that uses an aluminum heat sink. This structure eliminates the need for the base plate and thermal grease by solder bonding the insulating substrate and aluminum heat sink, resulting in successful reduction of thermal resistance by 30%. By using aluminum for the heat sink, the mass has been reduced to 1/3 of the existing structure of a copper heat sink, and corrosion resistance against long life coolant (LLC) has also been achieved.

3.2 Technical issues with adoption of aluminum heat sink

This product is an all-in-one package and, for preventing thermal coupling between IGBTs due to high integration, improvement in cooling performance is required. Table 1 shows the fundamental physical properties of the insulating substrate and heat sink materials. Aluminum has 1.5 times larger thermal expansion coefficient than copper. This causes higher stress to be applied on the solder bonding between the aluminum heat sink and insulating substrate than the conventional product, and hence further strength enhancement was necessary. There are two issues to overcome for realizing a direct liquid cooling structure using a lightweight aluminum heat sink:

(a) Improvement in cooling of aluminum heat sink
(b) Solder life time of thermal cycling test

In order to solve these issues, we have attempted to improve the cooling design technology and developed a high-strength solder.

4. Cooling Design of Aluminum Direct Liquid Cooling Structure

4.1 Relation between IGBT chip temperature and coolant temperature

In a liquid cooling structure, heat generated from IGBTs and FWDs is dissipated from the coolant through the module material and heat sink. Figure 4 shows the relation between the IGBT chip temperature and coolant temperature.

The IGBT chip temperature is highly dependent on the coolant temperature and is less correlated with the flow rate change. That is, lowering the coolant temperature is more effective than increasing the flow rate

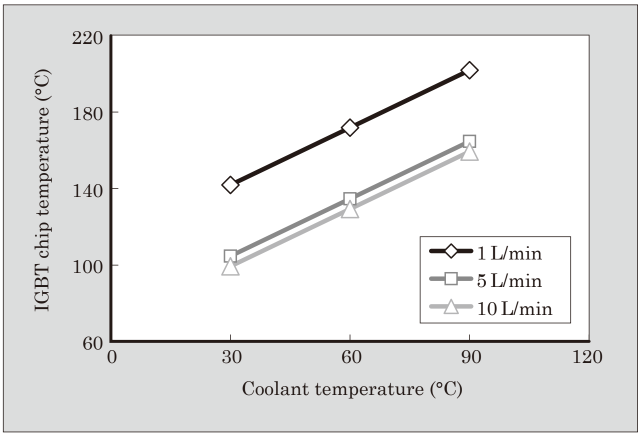

Fig.4 Relation between IGBT chip temperature and coolant temperature

of the coolant that flows through the heat sink to lower the IGBT chip temperature, or reducing the thermal resistance.

4.2 Flow channel design

It has been clear that the temperature of the coolant under the IGBT chips has an influence on the cooling performance and we have used a flow channel design with the coolant temperature taken into account.

Figure 5 shows heat sink and flow channel configuration examples. Type A is a structure in which the coolant flows in the longer direction with reference to the cooling unit. Meanwhile, Type B has a structure with the coolant flowing in the shorter direction and the number of devices that can be arranged for a coolant flow is less than that of Type A. The fewer the number of devices, the smaller the temperature increase of the coolant.

The structure that allows the device temperature to be lowered more is Type B, which coincides with the thermo-fluid analysis result. Making the cooling unit wider as in Type B allows the pressure loss of the heat sink to be reduced. The rate of flow in the cooling unit is inclined to be uneven, and we prevented this by optimizing the cooling structure.

4.3 Optimization of flow rate distribution

For improving the cooling performance, it is important to improve the heat exchange performance of the cooling fins not only by keeping the coolant at low temperature but also by increasing the flow rate. This

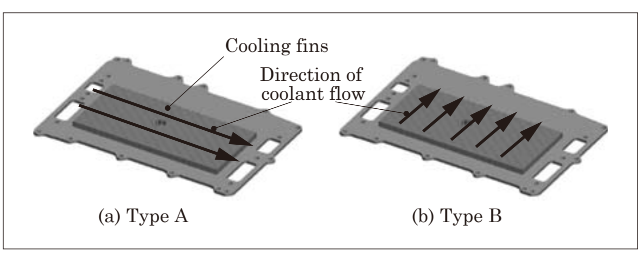

Fig.5 Example of heat sink and flow channel configuration

product is a module integrating three functions and the respective function has different maximum heat generation condition. Accordingly, we attempted to improve the cooling performance by providing optimized distribution of the coolant according to the heat generation distribution of each IGBT.

Figure 6 shows an image of the flow rate distribution of the coolant flowing in the heat sink. The rates of flows between fins are indicated by arrows. Before improvement, as shown in Fig. 6 (a), the flow resistance decreases and the flow rate increases as the distance from the inlet becomes longer. With this product, the heat generation density of PDU1 is higher than those of PDU2 and VCU. It is necessary to increase the flow rate of the coolant in a portion with a higher heat generation density. In order to adjust the flow rate distribution of the cooling unit, we have provided resistors in the channel as appropriate, as shown in Fig. 6 (b). This has allowed the flow rate distribution to be controlled according to the heat generation density[1].

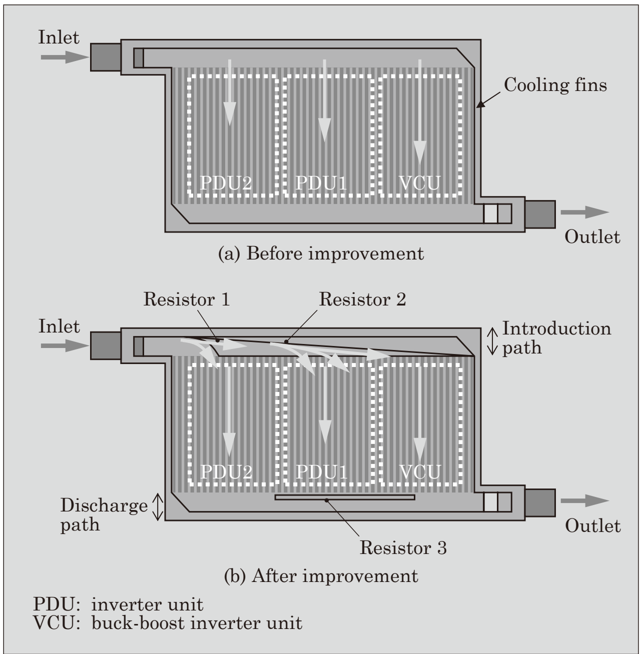

Fig.6 Image of coolant flow rate distribution

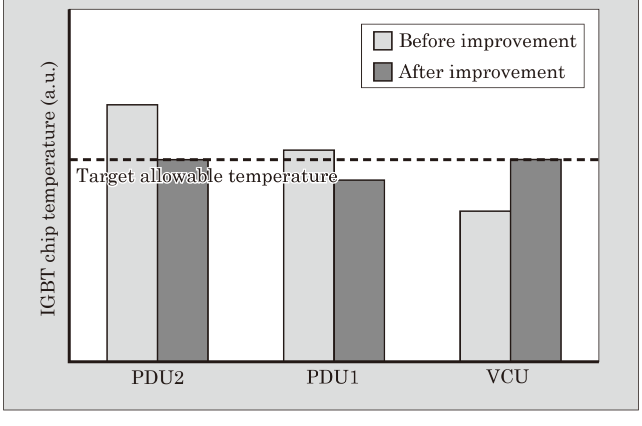

Fig.7 IGBT chip temperature before and after optimization

Figure 7 shows a comparison of IGBT chip temperature before and after the optimization. The temperature of each device has been averaged to equal to or lower than the target allowable temperature of the device by optimizing the flow rate distribution[2].

5. High-Strength and High-Reliability Solder

The thermal expansion coefficient of aluminum, which constitutes the heat sink material, is 23.5 ppm/K, or approximately 1.4 times that of copper, and the stress on the solder layer increases. To address this issue, we have developed a high-strength solder that ensures the service life required for in-vehicle products.

5.1 Development concept

Figure 8 shows a schematic diagram of the solder structure after a reliability test. It illustrates changes of the microstructure of solid solution strengthening and precipitation strengthening under high temperature, as metal strengthening mechanisms. Conventionally, solders using a single strengthening mechanism have been used. For even higher reliability, we worked on developing a high-strength solder that combines two strengthening mechanisms.

For the development, commonly used Sn (tin) has been selected as the base material and, Sb (antimony), which has been proven as material effective for improving mechanical characteristics and heat resistance, has been selected as the second element. With the additive amount of Sb with reference to Sn equal to or smaller than the solid solubility limit, solid solution strengthening is expected to become effective[3]. In addition, when the additive amount of Sb is increased to higher than the solid solubility limit, an SnSb compound that cannot dissolve will separate. Simultaneous appearance of two mechanisms of strengthening, namely solid solution strengthening and precipitation strengthening, gives rise to expectations for suppressing grain boundary cracking[4, 5].

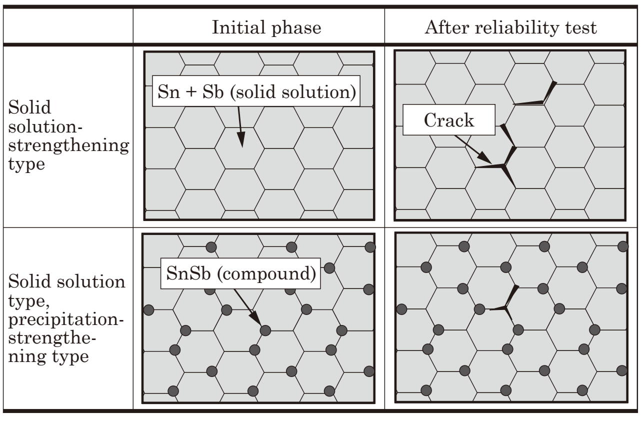

Fig.8 Schematic diagram of solder structure after reliability test

Based on this idea, we have verified the influence of the additive amount of Sb on the solder material characteristics.

5.2 Influence of Sb additive amount on solder strength

In order to demonstrate the development concept described in Section 5.1, we have conducted strengthening evaluation on two types of Sn-Sb solders with different additive amounts of Sb: Type 1 and Type 2. With Type 1, the additive amount of Sb was adjusted to equal to or smaller than the solid solubility limit with reference to Sn. With Type 2, the additive amount of Sb was adjusted to larger than the solid solubility limit.

Figure 9 shows the results of tensile tests using solders Type 1 and Type 2. The tests were conducted under room temperature conditions with JIS-compliant specimens molded by casting them into the respective compositions. Based on the results, we have confirmed that Type 2, which added more Sb than the solid solubility limit, presented strength at least 1.5 times that of Type 1, and we confirmed that strength enhancement can be realized by precipitation strengthening.

Then, in order to evaluate the heat resistance of solder Type 2, we examined the strength change after high-temperature aging*2 by simulating the actual operating environment. Figure 10 shows the tensile strength after high-temperature storage as compared with the initial strength. In this examination, Sn-Ag solder, which is a representative precipitation-strengthening solder, is used for comparison.

Type 2 solder maintains the initial strength after 1,000 hours at both 150 °C and 175 °C. Meanwhile, the Sn-Ag solder had its strength in a high-temperature environment reduced by approximately 40% as compared with the Sn-Sb solder (Type 2).

As a result of this, we have confirmed that combining solid solution strengthening and precipitation strengthening provides excellent strength in high-temperature conditions and satisfactory heat resistance.

Then, we carried out reliability evaluation on Type 2.

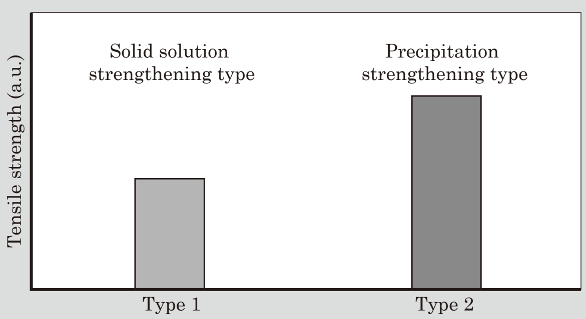

Fig.9 Comparison of tensile strength of Sn-Sb solder

*2: Aging: a phenomenon in which metallic properties (for example hardness) change over time.

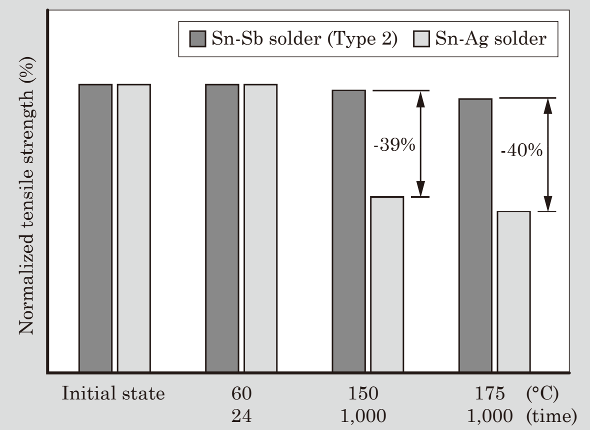

Fig.10 Tensile strength after high-temperature storage test

5.3 Reliability evaluation of Sn-Sb solder

We made specimens with the insulating substrate solder-bonded to an aluminum plate and carried out temperature cycle lifetime evaluation. The test was conducted under the conditions of −40 to +105 °C for temperature cycle evaluation and the crack length was imaged by a scanning acoustic tomograph (SAT) for measurement.

As result of comparing Sn-Sb and Sn-Ag solders, Fig. 11 shows SAT images of solder bonding after 2,000 cycles in the temperature cycle test, and Fig. 12 shows

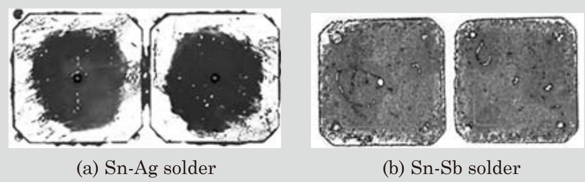

Fig.11 SAT images of solder bonding after temperature cycle test

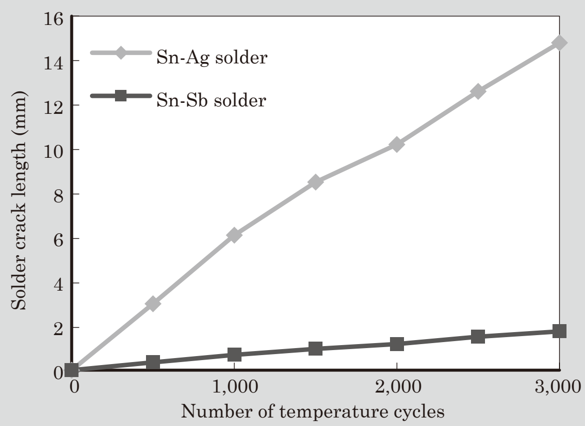

Fig.12 Crack length increase in temperature cycle test

the crack length increase of the respective solders in the temperature cycle test.

The SAT images show areas with cracks progressing in white. Specimens that use the Sn-Sb solder show only minor progress of cracks. On the other hand, a noticeable progress of cracks is observed in specimens that use the Sn-Ag solder. Accordingly, the Sn-Sb solder has been confirmed to have higher durability than the Sn-Ag solder.

We have, therefore, made it clear that the developed Sn-Sb solder ensures high reliability in bonding between the insulating substrate and aluminum heat sink, which have significantly different thermal expansion coefficient.

6. Postscript

This paper has outlined the intelligent power module (IPM) for hybrid vehicles and described two packaging technologies.

Packaging technologies support customers with inverter development and design. We intend to use these technologies as the basis for working on further technological innovation to offer products that contribute to high efficiency and energy conservation.

References

(1) Gohara, H. et al. Cooling device for semiconductor module and semiconductor module. Patent Application. PCT/JP2012/072554.
(2) Saito, K.; Otuka, H. "Development of PCU for a new HEV drive". Proceedings of Japan Society of Automotive Engineers Annual Congress (Spring). Kanagawa, Japan, 2013.
(3) Nishiura, A, Morozumi, A. "Improved life of IGBT module suitable for electric propulsion system". Proceedings of the 24th EVS, Stavanger, 2009.
(4) Morozumi, A. et al. "Direct Liquid Cooling Module with High Reliability Solder Joining Technology for Automotive Applications". Proceedings of the 25th ISPSD & ICs, Kanazawa, 2013.
(5) Saito, T. et al. "New assembly technologies for Tjmax=175°C continuous operation guaranty of IGBT module". Proceedings of PCIM Europe 2013, Nuremberg, p.455-461.

Fuji Electric
Innovating Energy Technology